Journal of the Korean Society for Nondestructive Testing
Vol. 30, No. 3 (2010. 6)

Characteristics on Temperature Evolution in the Metallic Specimen by Ultrasound-Excited Thermography

M. Y. Choi*, J. H. Park*, K. S. Kang** and W. T. Kim***†

Abstract In ultrasound-excited thermography, the injected ultrasound to an object is transformed to heat and the appearance of defects can be visualized by thermography camera. The advantage of this technology is selectively sensitive to thermally active defects. Despite the apparent simplicity of the scheme, there are a number of experimental considerations that can complicate the implementation of ultrasound excitation thermography inspection. Factors including acoustic horn location, horn-crack proximity, horn-sample coupling, and effective detection range all significantly affect the detect ability of this technology. As conclusions, the influence of coupling pressures between ultrasound exciter and specimen was analyzed, which was dominant factor in frictional heating model.

Keywords: Ultrasound Excited, Infrared Thermography, Heat Generation Mechanism, Thermoelasticity, Friction Fatigue Crack

1. Introduction

As shown in the Fig. 1, the ultrasound infrared thermography technology is the technology used for detecting the defect by measuring the heat generated in the defective area when projecting the ultrasound with band of 20~30 kHz on object (Favro et al., 2001). This technology enables its user to inspect the wide area and detect the defects such as crack or separation in the real time, so it is highlighted as a next generation nondestructive inspection technology in the automobile industry and aerospace industry (Meyendorf et al., 2002). In this technology, the heat generation mechanism resulted from the ultrasonic excitation is not clearly understood. It is believed that the thermo-mechanical coupling effect and friction between defective interfaces are contributed as the main causes for the ultrasound excitation (Han et al., 2004; Rothenfusser, 2005). In this study, we establish the numerical model of temperature evolution based on the thermo-mechanical coupling effect and the friction effect, respectively and in experiment our assumption is verified by inspecting the fatigue crack of compact tensile specimen.

2. Temperature Evolution Analysis

The ultrasound generator with the output of above 1 kW and the frequency of 20 or 30 kHz is generally used in this technology. When the high power ultrasound is injected on the object,

Received: November 8, 2009. Revised: January 29, 2010; April 20, 2010, Accepted: June 10, 2010. *Safety Metrology Group, Korea Research Institute of Standards and Science, Daejeon 305-600, Korea, **Measurement Technology Development Team, Hyundai Steel Co., Dangjin, Chungnam 343-711, Korea, ***Major of Mechanical System Engineering, Kongju National University, Cheonan, Chungnam 331-717, Korea, †Corresponding Author: kwt@kongju.ac.kr

there are three basic modes of crack tip deformation, the opening (Mode I), the in-plane shear (Mode II), and the out-of-plane shear (Mode III) as shown in Fig. 2 (Homma et al., 2006). If reviewing this phenomenon in terms of heat generation mechanism, for the Mode I, stress is intensively generated at peak of crack and thermo- mechanical coupling effect is presumed as the main cause for the heat generation. For the Mode II (internal shear type) and Mode III (external shear type), heat generation is mainly caused by the friction between interfaces instead of stress concentrated at peak of crack. Therefore, the temperature change at crack is expressed as eqn. (1) based on two heat generation factor. Here, the loss resulted from the heat exchange are neglected.

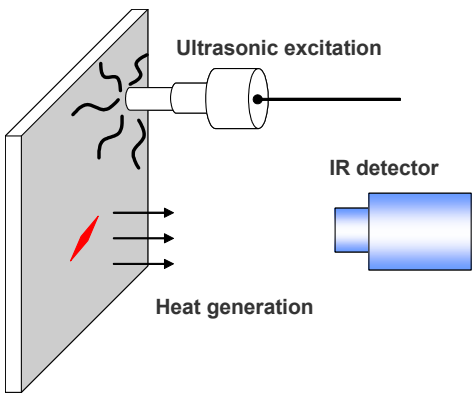

Fig. 1 Ultrasound-excited infrared thermography

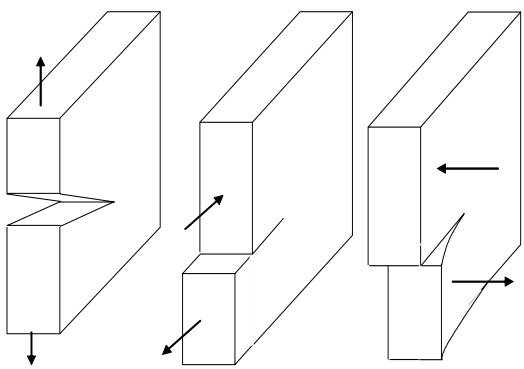

(a) Mode I (b) Mode II (c) Mode III

Fig. 2 Deformation modes at crack tip

$$\triangle T = T_M + T_F \quad (1)$$

Here $\triangle T$, T_M and T_F indicate the total temperature change at crack, temperature change resulted from the thermo-mechanical coupling effect and temperature change resulted from the friction respectively.

2.1 Thermo-Mechanical Coupling Effect

The temperature change resulted from the thermo-mechanical coupling effect (T_M) may be expressed as shown in eqn. (2) with classified into the temperature change (T_E) in the elastic deformation and temperature change (T_P) in the plastic deformation.

$$T_M = T_E + T_P \quad (2)$$

If the ultrasonic output, the contact area of ultrasonic excitation horn and the transmission efficiency up to the crack are presumed as 1 kW, 314 mm^2 and 100% respectively, the sound intensity of 12.7 W/mm^2 will be transferred. Also, this sound intensity is converted into the stress, 0.07 MPa. Since this value is too small for the yielding stress of metal material, the heat generation effect of plastic deformation may be disregard as shown in eqn. (2). Also, the temperature change in the elastic deformation (T_E), known as the thermoelastic effect, (Choi et al., 2006; Kim et al., 2008) is expressed as eqn. (3).

$$T_E = -K_m \cdot T_a \cdot \triangle \sigma \quad (3)$$

Here, K_m, T_a and $\triangle \sigma$ indicate the thermoelastic coefficient, surrounding temperature and change in the sum of the principle stresses, respectively. If the stress change ($\triangle\sigma$) in eqn. (3) is expressed by sinusoidal harmonic function ($\triangle\sigma\cos wt$), the heat generation resulted from the ultrasonic excitation during time, τ may be expressed as shown in eqn. (4).

$$T_E = -K_m \cdot T_a \cdot \frac{1}{\tau}\int_0^{\tau} \triangle\sigma \cos wtdt \qquad (4)$$

In the hypothetic case of an elastic material subjected to uniaxial stress and exhibiting no damping, $\sigma(t) = E\varepsilon(t)$, the stress-strain diagram is linear and the integration term is equal to zero (Blok, 1987). However, for a realistic elastic material under the same conditions the time dependence shows an additional phase shift, $\sigma(t) = E\varepsilon(t+\theta)$. This process is the irreversible process where the released energy per cycle is converted into the thermal energy, so it may be expressed as shown in eqn. (5).

$$T_E = -K_m \cdot T_a \cdot \frac{1}{\tau}\int_0^{\tau} f \cdot \eta \cdot \left(\int_{\varepsilon_1}^{\varepsilon_2} Ed\varepsilon - \int_{\varepsilon_2}^{\varepsilon_1} Ed\varepsilon\right)dt \qquad (5)$$

Here, η, f, E and ε indicate the energy conversion efficiency, ultrasound frequency, elastic modulus and strain respectively. If the released energy is presumed as the maximum between elastic coefficient and strain, it may be expressed as $\int_{\varepsilon_1}^{\varepsilon_2} Ed\varepsilon - \int_{\varepsilon_2}^{\varepsilon_1} Ed\varepsilon = E\varepsilon^2$, so eqn. (5) may be rewritten as eqn.

$$T_E = -\eta \cdot K_m \cdot T_a \cdot f \cdot \frac{1}{\tau}\int_0^{\tau} E \cdot \varepsilon(t)^2 dt \qquad (6)$$

If the stress amplitude resulted from the ultrasonic excitation, ultrasonic excitation frequency, excitation duration, ambient temperature and energy conversion efficiency are presumed as 0.07 MPa, 30 kHz, 10 s, 300 K and 100% respectively, temperature change of carbon steel materials may be estimated as shown in the (Table 1) based on eqn. (6). The temperature change resulted from the ultrasonic excitation is too small to be neglected, even if the stress concentration coefficient is considered. As a result, thermo-mechanical coupling effect of eqn. (1) does not contribute to the heat generated at crack.

Table 1 Temperature change resulted from the thermoelasticity

Materials	K_m (Pa-1)	E(GPa)	$\triangle T$(K)
SAE 1045	3.01×10^{-12}	205	6.5×10^{-6}
Al 7075-T6	9.34×10^{-12}	72	5.7×10^{-5}

2.2 Frictional Effect

If the thermo-mechanical coupling effect does not contribute to the heat generation of crack and friction between interfaces is acted as the main cause of heat generation, heat generation resulted from the friction between two interfaces is expressed as shown in eqn. (7).

$$q = \mu \cdot P \cdot \upsilon_S \qquad (7)$$

Here, μ, P and ν_S indicate the friction coefficient, contact pressure and friction velocity respectively. The maximum temperature change resulted from the friction between interfaces under relative motion may be express as shown in eqn. (8) (Block, 1987).

$$T_{\max} = C\frac{\mu\, p\left|\sqrt{\upsilon_1} - \sqrt{\upsilon_2}\right|}{\sqrt{b}\sqrt{k\,\rho\, c_p}} \qquad (8)$$

Here, C, p, ν, b, k, ρ and c_P indicate the shape coefficient, contact force for a length, particle velocity, contact length, coefficient of heat conduction, density and specific heat at constant pressure, respectively. In eqn. (8), p can be expressed in the form of $p = p_0 \cos wt$ in case of ultrasonic excitation, and if the relative velocity between two interfaces is constant during the ultrasonic excitation time, τ and constant pressure is generated on the friction side, the equation may be rewritten as follows:

$$T_{\max} = C\, f \frac{\mu\, p_0 \sqrt{\upsilon_1}}{\sqrt{b}\sqrt{k\rho c_p}} \int_0^{\tau} \cos \omega t dt \qquad (9)$$

This equation shows the temperature change depends on the frequency and pressure of the induced ultrasound. The ultrasound with 30 kHz frequency and 1 kW output excites aluminum alloy with 11 mm length fatigue crack in temperature change, 8 K, which is enough to be distinguished with infrared thermography (Choi et al., 2006).

3. Experimental Set-up

The test equipment for ultrasound-excited infrared thermography was setup inside the adiabatic chamber to minimize the heat exchange between specimen and external heat source as shown in the Fig. 3(a). Ultrasound excitation system was with output of 400 W and frequency of 30 kHz and infrared camera (NEDT: 20 mK) is manufactured by the Cedip Co.. A crack was implemented by performing the fatigue test against the specimens such as aluminum alloy steel and carbon steel CT and then measure the length and width of crack using the optical microscope (Kim et al., 2006). The test side and excitation side was set to be same for the ultrasound-infrared thermography test as shown in the Fig. 3(b) and the fatigue crack generated in the notch area for the test was detected (Kim and Choi, 2008).

4. Discussion

4.1 Detecting the Fatigue Crack in the Specimen Made of Aluminum Alloy Steel

From this experiment, for the purpose of defining the heat generation mechanism in the fatigue, it was performed the fatigue test against

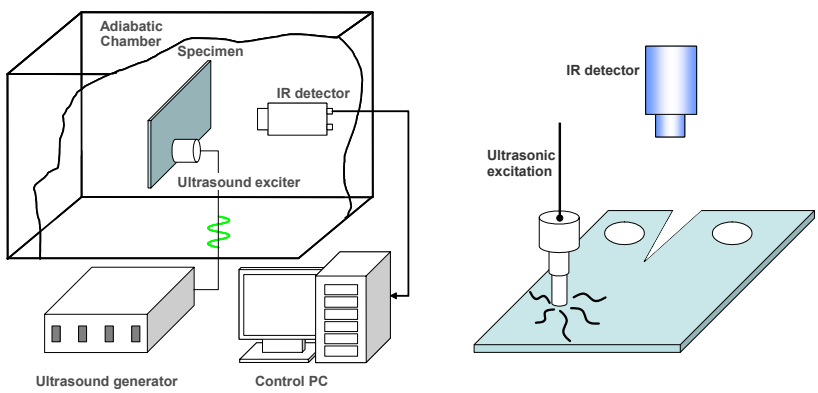

Fig. 3 Experimental configuration; (a) Inspection system configuration, (b) Inspection area

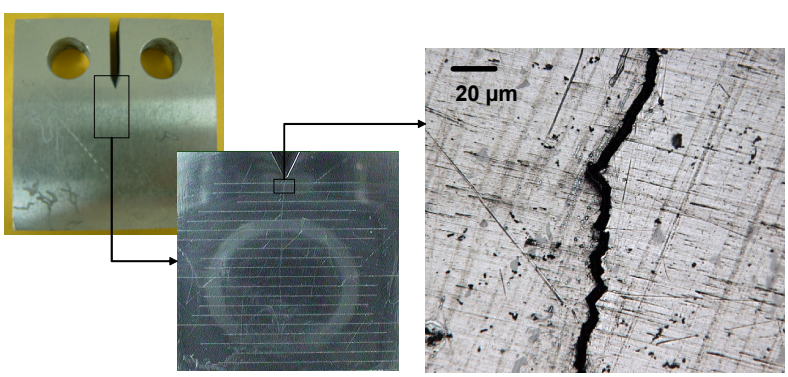

Fig. 4 Microscopic images of fatigue crack of aluminium alloy

the CT Specimen made of aluminum alloy steel crack, and the width and length of fatigue crack was measured. Then, the length and width for defects with results of ultrasound-excited infrared thermography were compared. The Fig. 4 shows the fatigue crack of aluminum alloy steel. The length and width of crack measured using the optical microscope were 17 mm and 2.1 ~ 10.9 μm respectively.

The crack was detectable within 1 second after the ultrasonic excitation. At positions showing the maximum temperature change, results measured was compared. The Fig. 5(a) and (b) show the thermography image before the ultrasonic excitation and the thermography image when the biggest temperature change is measured after the excitation. The Fig. 5(b) shows the temperature distribution along the length of crack and the results of measuring the width of crack in each position. The width of crack was measured as 10.9 μm and 2.1 μm at start and peak points, respectively. The temperature difference between position without crack and position showing the biggest temperature change was measured as 5.1℃. The test results show that the heat generates in whole crack. If the elastic effect is functioned or acted as the main cause for the heat generation, heat will be generated at peak of crack. However, the test results show that the biggest heat is generated in position where the widest crack is measured (10) instead of peak of crack. These results prove or show that the friction is the main factor of heat

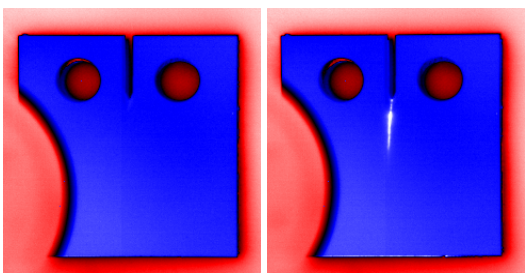

(a) (b)

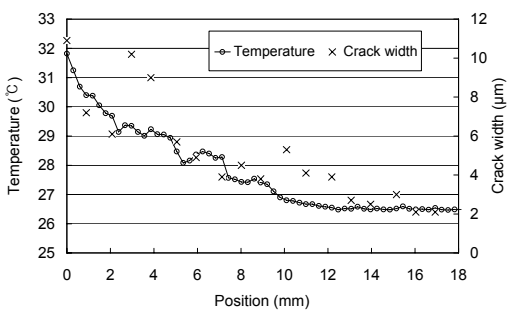

(c)

Fig. 5 Fatigue crack inspection of aluminum alloy; (a) Before inspection, (b) Maximum heat generation, (c) Temperature and crack width along crack length

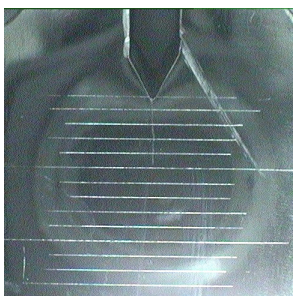

Crack length (mm)	Crack width (μm)
0	9.8
1	9.6
2	5.6
3	5.6
4	5.6
5	5.6

(a)

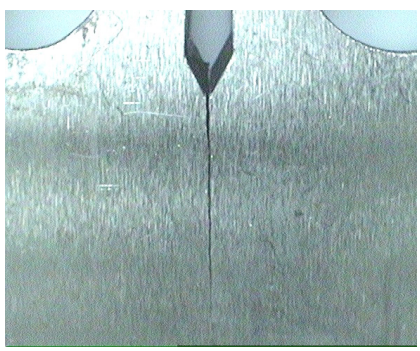

Crack length (mm)	Crack width (μm)	Crack length (mm)	Crack width (μm)
0	337.4	9	186.5
1	294.3	10	158.6
2	275.2	11	150.4
3	246.7	12	155.2
4	237.5	13	136.8
5	226.2	14	148.9
6	194	15	80.2
7	188.3	16	46.3
8	190.3	17	40.2

(b)

Fig. 6 Fatigue crack inspection of carbon steel; (a) Microscope image and crack width of specimen A, (b) Microscope image and crack width of specimen B

generation as advocated in this paper. Also, the inspection image of Fig. 5(b) shows that the length of crack is 11 mm (size of actual crack is 17 mm). The temperature distribution is measured as 31.8℃ and 26.7℃ at start point and end point, point of being 11 mm away from the start point, respectively. The width of crack is measured as 10.9 μm and 4.1 μm at temperatures of 31.8℃ and 26.7℃ respectively. This result shows that the sufficient load causing the friction is not transmitted because of narrow crack if the width of crack is less than 4 μm.

4.2 Detecting the Fatigue Crack from the Carbon Steel Specimen

Two carbon steel specimens showing the different width of crack were used for the inspection or test. The Fig. 6 shows the photo on actual crack of each specimen and change of width according to length of crack. The crack length and width of specimen A shown in the Fig. 6(a) are 5 mm and 5.6 ~ 9.8 μm. The crack of specimen B shown in the Fig. 6(b) is visually identifiable. The crack length and width of specimen B are 17 mm and 40.2 ~ 337.4 μm.

The Fig. 7 shows the results of ultrasound-infrared thermography inspection or test. While the results of test performed against the specimen A showed that the heat is generated at crack, results of test performed against the specimen B showed that no heat is generated at crack before and after the ultrasonic excitation. This result shows that no heat is generated because the contact force is not sufficient when the crack width is wide. Also, while the Fig. 7 (a) shows that the biggest heat is generated at peak of crack, the Fig. 7(b) shows that no heat is generated at peak of crack. This result shows that the heat resulted from the thermo-elasticity is not generated in the fatigue crack. The Fig. 8 is a graph showing the temperature change along the crack length of the specimen A. The average temperature of surface was measured as 21℃. This figure shows that the temperature is 1℃ increased at crack. If the distance between 2 peaks is presumed as the length of crack in the temperature distribution, the length of crack is measured as about 5 mm when measuring the length of crack using the ultrasound-infrared thermography. This result is same as the one measured using the optical microscope. We review the heat generation characteristics of

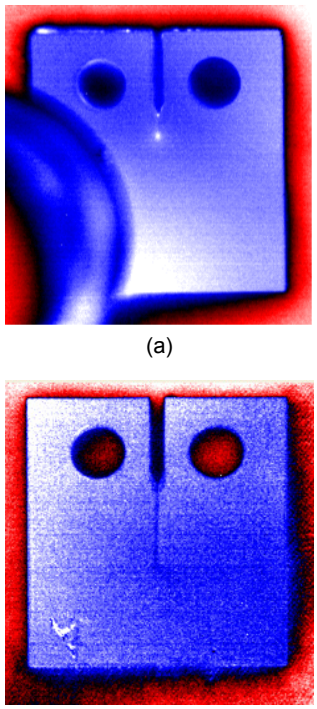

(a)

(b)

Fig. 7 Thermography inspection result; (a) Carbon steel specimen A, (b) Carbon steel specimen B

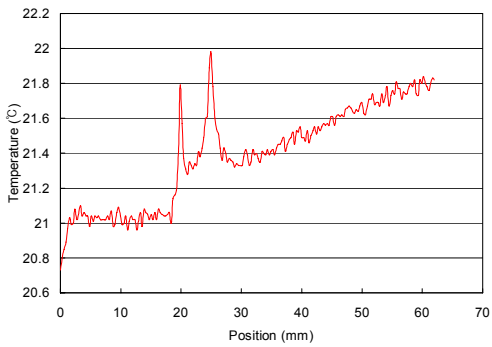

Fig. 8 Temperature of specimen A measured along crack length

aluminum alloy material and carbon steel. The reviewed results show that the heat generation characteristics are excellent if the crack width is between 5 ~ 10 μm. This result shows that the friction force stated in eqn. (7) is closely related to the output of ultrasonic excited system and crack width as well.

5. Conclusion

This paper considered the thermo-mechanical coupling effect and friction effect for the purpose of analyzing or defining the heat generation mechanism of nondestructive ultrasound-infrared thermography inspection technology. We prove that the friction effect makes a big contribution to the heat generation. The results of fatigue crack detection test show that the heat generation characteristics are changed according to crack width and heat generation resulted from the thermo-elastic effect is not observed at peak of crack. Also, if the friction is functioned or acted as the main factor of heat generation as advocated in this study, heat generation characteristics may be considerably improved according to mode of projected ultrasound.

References

Blok, H. (1987) Thermo-Tribology, *International Conference on Tribology*, Institution of Mechanical Engineers, London, UK, pp. 1-8

Choi, M. Y., Kang, K. S., Park, J. H., Kim, W. T. and Kim, K. S. (2006) Measurement of Defects and Stress by Infrared Thermography, *Journal of the Korean Society for Precision Engineering*, Vol. 23, No. 10, pp. 30-35

Favro, L. D., Thomas, R. L. and Han, X., Zhong, O., Newaz, G., and Gentile D. (2001) Sonic Infrared Imaging of Fatigue Cracks, *International Journal of Fatigue*, Vol. 23, pp. S471–S476.

Han, X., Zeng, Z., Li, W. and Islam, M. S. (2004) Acoustic Chaos for Enhanced Detect Ability of Defects by Sonic Infrared Imaging, *Journal of Applied Physics*, Vol. 95, No. 7, pp. 3792-3797

Homma, C., Rothenfusser, M., Baumann, J. and Shannon, R. (2006) Study of the Heat Generation Mechanism in Acoustic Thermography, in: D. O. Thompson and D. E. Chimenti (Eds.), *Review of Quantitative Nondestructive Evaluation*, Vol. 25, American Institute of Physics, New York, PP. 566-573

Kim, W. T., Choi, M. Y., Park, J. and Kang, K. S. (2008) Analysis of Thermoelastic Stress in the Cantilever Beam by Lock-in Thermography, *Journal of the Korean Society for Nondestructive Testing*, Vol. 28, No. 3, pp. 273-278

Meyendorf, N. G. H., Rosner, H., Kramb, V. and Sathish, S. (2002) Thermo-Acoustic Fatigue Characterization, *Ultrasonics*, Vol. 40, pp. 427-434

Rothenfusser, M. and Homma, C. (2005) Acoustic Thermography: Vibrational Modes of Cracks and the Mechanism of Heat Generation, in: D. O. Thompson and D. E. Chimenti (Eds.), *Review of Quantitative Nondestructive Evaluation,* Vol. 24, American Institute of Physics, New York, pp. 624-631